Effects of hydrodynamic pressure on the seismic responses of underground vertical shafts

***Bu Zhang[1] and †Zhiyi Chen[1,2]**

[1]Department of Geotechnical Engineering, Tongji University, Shanghai 200092, China
[2]Key Laboratory of Geotechnical and Underground Engineering of Ministry of Education, Shanghai 200092, China

*Presenting author: zhangbu@tongji.edu.cn
†Corresponding author: zhiyichen@tongji.edu.cn

Abstract

More and more deep drainage and storage pipeline systems play an important role in preventing urban flooding and waterlogging in urban 'sponge cities'. As the main structures in this systems, shafts are used to collect, reserve and transport the water. The effect of inner water on seismic response of a deep shaft is studied with three different levels of inner water: full, half, and empty. The hydrodynamic pressure is simulated with the CAS (coupled acoustics and structure) method which can consider not only the impulsive pressure effect, but also the convective pressure effect. Results present that the seismic displacement responses of shaft under different water levels are nearly consistent, while the shaft inner forces increase with the increase of the inner water level.

Keywords: Vertical shaft, Inner water, Coupled acoustics and structure method, Seismic Response

1. Introduction

With the construction and development of urban cities, especially the city resilience in controlling and preventing the city flood in heavy rainstorm, the construction of the sponge city gradually becomes a focus. The underground reservoir shaft, as a main underground structure and the important part of the sponge city project, is used to store up and discharge the water. Due to the non-renewable characteristic of underground space and the great difficulties in restore of the underground structure, the safety of reservoir shaft under earthquake excitation has become a rising concern.

Many researchers have studied the hydrodynamic distribution formulation of the aboveground tank under seismic excitation [1-3]. They assumed the tank as a rigid body with only translation motion. The added mass method was proposed to simulate the effect of hydrodynamic impulsive pressure on the above ground tank [4-6], which are usually neglected the effect of the connective pressure.

Simplified analytical method [7], experiment test [8] and numerical method [9-11] was used to explore the seismic performance of shallow underground tanks with inner water. And the results showed that the effect of the sloshing of inner water can be neglected, which is the same as the above ground tanks. However, as a vertical embedded structure, the shaft not only behaves with translation motion but also with rotational motion under earthquake excitation. Obviously, the effect of hydrodynamic pressure on the underground reservoir, especially on the shaft inner forces and dynamic displacements, should be further researched.

In order to simulate the dynamic responses of shaft inner water, the hydrodynamic pressure needs to be simulated accurately. The CEL (Coupled Euler and Lagrange), SPH (Smoothed Particle Hydrodynamic), and CAS (Coupled Acoustics and Structure) methods all can be used to simulate the dynamic behavior of inner water in detail. For the SPH method [12-14], the water is simulated as uniform distributed partials. However, the particles need to be intensive in order to obtain the accurate results. For the CEL method [15-17], the shaft is modeled as Lagrange element and the inner water is modeled with the Euler element; in order to simulate the water motion, the Euler elements need to be refined, which would increase the element number especially in 3D model. For the CAS method [17, 18], the Acoustics element with pressure DOF can be used to obtain the pressure of inner water, and the calculation efficiency is higher than the above two methods. Taking the calculation efficiency into account, the CAS method is efficient in simulating the sloshing and hydrodynamic behavior of inner water and shafts. Thus the CAS method is adopted in this paper.

In this paper, three cases with full water, half water, and no water have been simulated and the effects on the shaft displacement and inner forces distribution pattern has been investigated with CAS method.

2. Numerical modelling

2.1 Site and drainage shaft

Here in order to carry out parameter sensitivity analyses, a series of 3D dynamic time history analyses of shafts are performed with the large-scale commercial finite element software *ABAQUS* [19]. The model is shown in Fig. 1a. The model is 400 m in the horizontal directions, which is more than five times of the shaft diameter to prevent boundary-waves reflection. Because the wave velocity of the bottom soil layer is greater than 600 m/s, the bottom soil layer is considered as the bedrock; hence, the model is 120 m in the vertical direction. The depth of the shaft is 60 m and the baseboard thickness is 4 m. The thickness of shaft side wall is uniform along depth. Fig. 1b shows the model of inner water which simulated by the AC3D8R element. Fig. 1c shows the central cross-section of the shaft, in which the lining is simulated by S4R element and the baseboard is simulated by C3D8R element. The parameters of the shaft in drainage system are listed in Table 1.

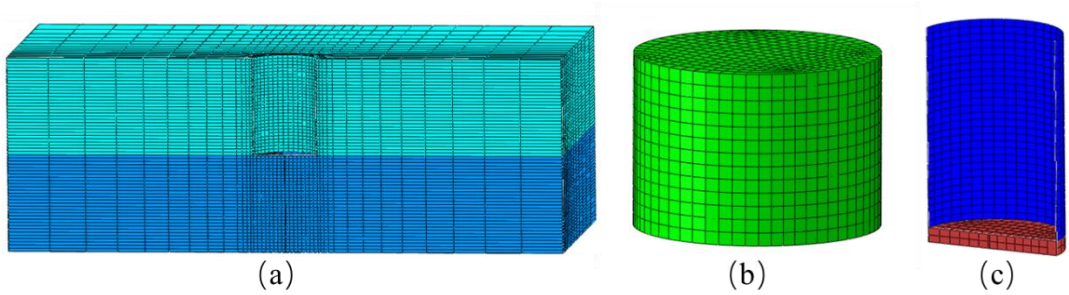

Figure 1. Schematic diagram of vertical section of the three-dimensional model: (a) vertical profile of surrounding soil; (b) inner water and (c) vertical profile of shaft

Table 1. Geometrical parameters of the shaft and surrounding soils

Name	Depth D (m)	Density ρ (kg/m^3)	Shear-wave velocity v_s (m/s)	Poisson's ratio u	Elasticity modulus E (MPa)
Soil-1	30	1850	250	0.3	300
Soil-2	30	1900	300	0.3	520
Shaft	60	2500	-	0.2	34500

2.2 Inner water

The inner water is simulated by the Acoustics element AC3D8 with pressure DOF. In this model, three different water levels are considered. The height of water level in each case is 0, 28m, 56m, respectively. The detail parameters of inner water are listed in Table 2.

Table 2. Parameters of inner water

Calculation Cases	Water Depth H (m)	Density ρ_w (kg/m^3)	Dynamic viscosity μ(N sec/m^2)	Bulk modulus K (MPa)
No water	0			
Half water	28	1000	0.001	2140.4
Full water	56			

2.3 Boundary conditions

MPC boundary conditions are obtained for lateral boundary conditions in the dynamic procedure, allowing it to move as a free field. The boundary at the model top is free. The vertical degree of the model base is fixed, while the input seismic motion is applied in horizontal direction.

For the inner water, the impedance boundary conditions are applied for the free surface in order to simulate the effect of the sloshing effect. The acoustic particle velocity in the outward normal direction of fluid surface, $\dot{u}_{out}$, is related to the pressure as well as the change rate with time of pressure as follows:

$$\dot{u}_{out} = \frac{1}{k}\frac{\partial p}{\partial t} + \frac{1}{c}p \tag{1}$$

where, p is the acoustic pressure, $1/k$ is the proportionality coefficient between the pressure and the displacement in normal direction to the surface, and $1/c$ is the proportionality

coefficient between the pressure and the velocity in normal direction to the surface ($1/k=1/\rho_w g$, $1/c=0$) [17-19].

2.4 Input seismic motion

An artificial earthquake motion for Shanghai is input horizontally from the model base. Fig. 2 shows the time history of the seismic excitation signal and its Fourier spectrum. The ground motion is uniform without taking the wave travelling effects into account. The ground motion has a duration of 20 s with a maximum value of 0.1g. The frequency is mostly between 0 and 10 Hz.

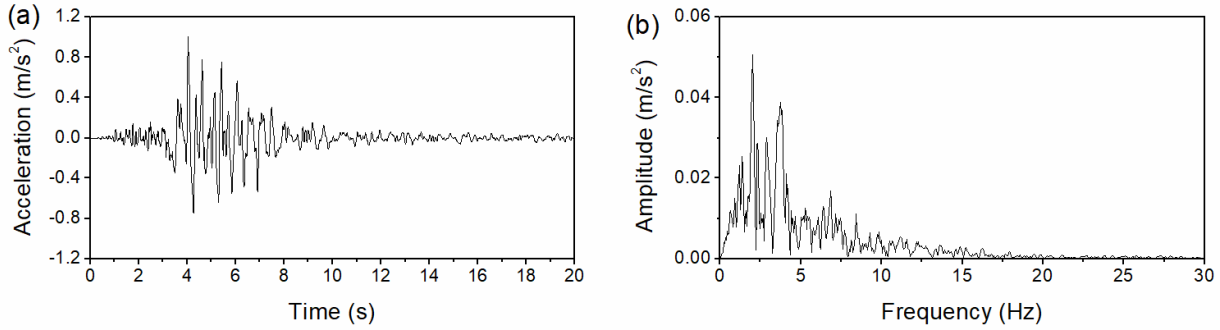

Figure 2. (a) Acceleration time history curve and (b) Fourier amplitude of the Shanghai artificial earthquake motion

3. Results and discussion

3.1 Sloshing displacement

In the FEM model, the acoustic pressure is obtained directly at the top surface of the liquid and the sloshing displacement, *h*, can be obtained by using the correlation formulation [17]:

$$h = \frac{p}{\rho_w g} \tag{2}$$

where, p is the hydrodynamic pressure of free surface, ρ_w is the density of water, g is the gravity acceleration.

Fig. 3 shows the sloshing displacement time history response of the water free surface. A probe is placed on the initial free surface connecting the shaft right side wall. Compared with the shaft sloshing displacement, the sloshing tendency is nearly the same. It can be seen that maximum sloshing displacement amplitude is 10 cm for the full water case, while the maximum sloshing displacement amplitude is 6 cm for the half water case. The magnitude of the sloshing displacement is relatively small compared with the inner water height.

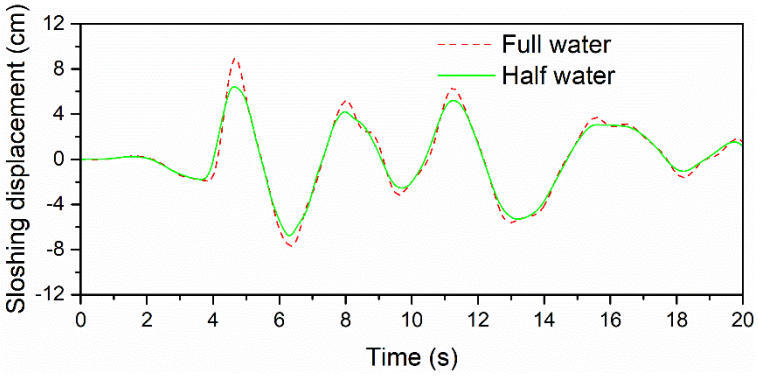

Figure 3. Sloshing displacement time-history responses of the shaft subjected to earthquake ground motions

3.2 Distribution of hydrodynamic pressure

The maximum hydrodynamic pressure distribution pattern is extracted at the time t=6.84s, when the magnitude of the shaft bottom acceleration reaches the maximum. In order to represent the distribute pattern, Fig. 4 shows the distribution of normalized hydrodynamic pressure along the height of the shaft. From Fig. 4 it can be seen that the normalized hydrodynamic pressure in both the full water and half water cases are nearly the same, while the negative magnitude at the top in the full water case indicates the effect of the convective pressure.

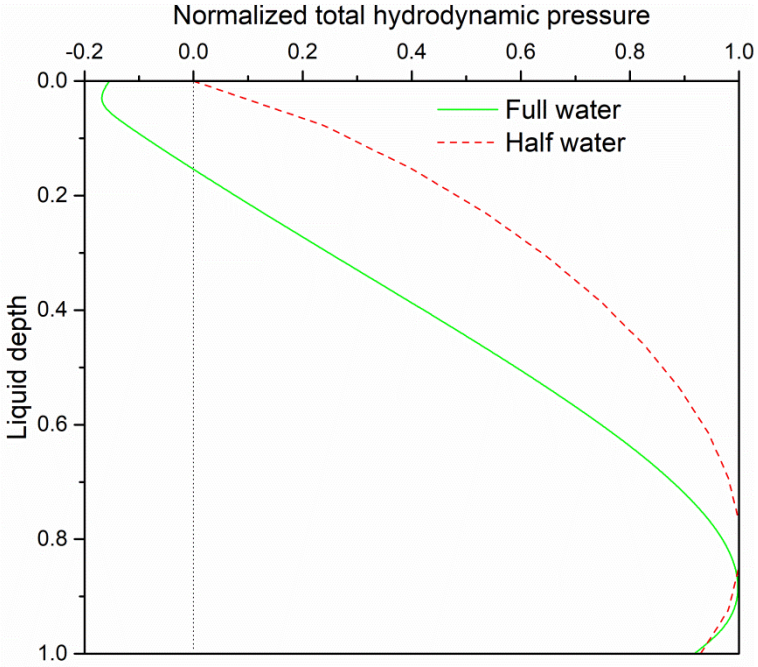

Figure 4. Normalized hydrodynamic pressure in shaft

3.3 Shaft displacements

In order to investigate the effect of inner water on shaft displacement, displacement history curves of the shaft bottom and top in three cases are compared in Fig. 5. It can be seen from Fig. 5a, the shaft bottom displacement curves in three cases are nearly the same, so are the shaft top displacement curves (Fig. 5b). It can be seen that effect of inner water on the shaft's

dynamic displacement can be neglected. At the same time, it also indicates that the shaft's dynamic displacement is mainly determined by the surrounding soils.

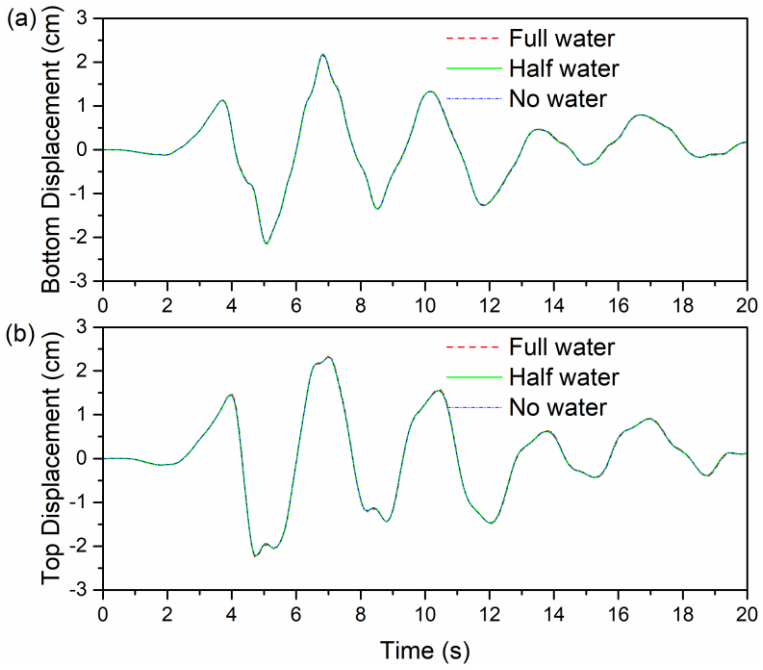

Figure 5. Shaft displacement time-history responses of the shaft:

(a) shaft bottom; (b) shaft top

3.4 Shaft inner forces

Fig. 6 shows the envelope distribution pattern of the circumferential bending moment, M_{cs}, and the circumferential axial force, T_{cs}, along the shaft depth in the cross-section of the shaft hoop. Calculation results of the three cases show that as the shaft inner water level increases, the circumferential inner forces of the shaft decrease also increases. This is because as the shaft water level increases, the hydrodynamic pressure increases, and the seismic load on the shaft lining increases finally.

Fig. 7 shows the envelope distribution pattern of the vertical bending moment, M_{as}, and the vertical axial force, T_{as}, along the shaft depth. Calculation results of the three cases show that as the shaft inner water level increases, the vertical inner forces along the depth increase. This is also because as the shaft water level increases, the hydrodynamic pressure increases, and the seismic load on the shaft lining increases finally.

From the perspective of the inner forces of the structure, the magnitude of the inner forces are nearly the same and there is no obvious effects on the shaft inner forces. As the shaft inner water level increases, the inner forces of the shaft lining increase with the shaft inner water level.

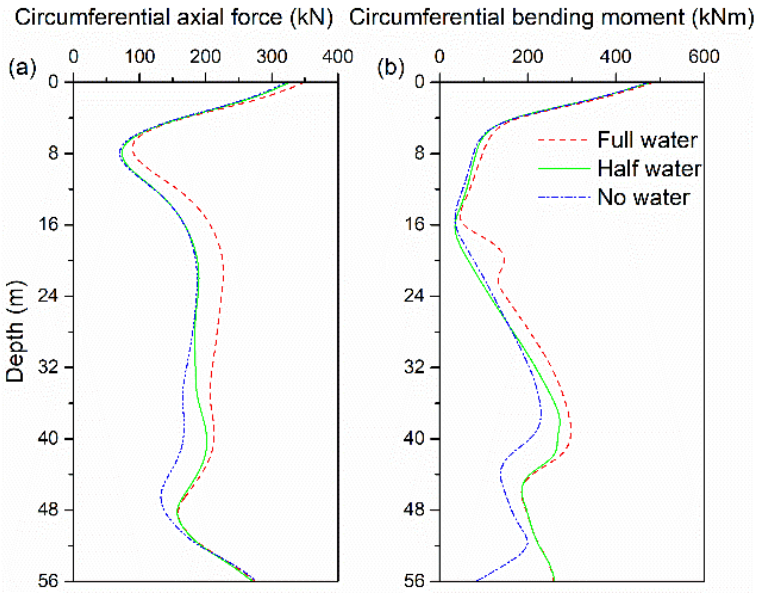

Figure 6. Envelopes of maximum internal forces in circumferential direction: (a) axial force; (b) bending moment

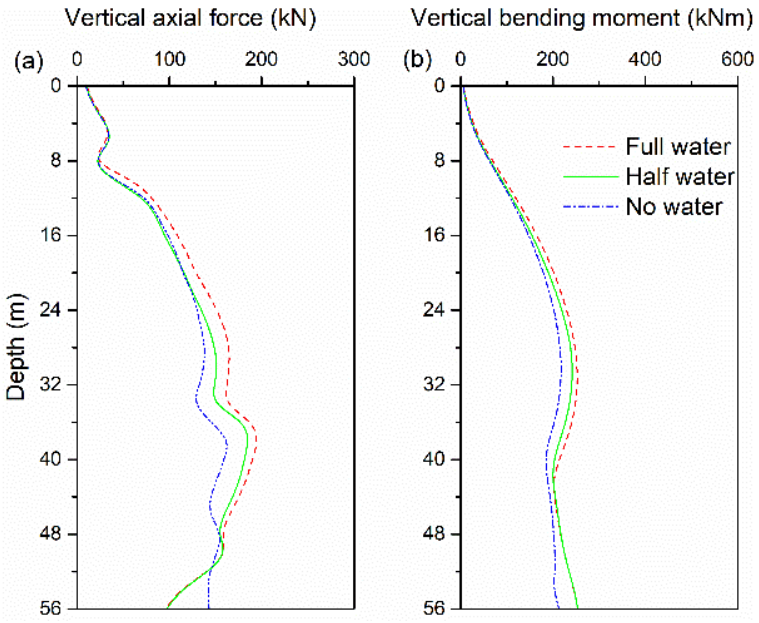

Figure 7. Envelopes of maximum internal forces in vertical direction: (a) axial force; (b) bending moment

4. Conclusions

The hydrodynamic effects of inner water on the shaft seismic responses are investigated in this paper through 3D CAS dynamic time history analysis with different inner water levels. The main conclusions are listed as follows:

- The inner water sloshing displacement is small, which is not the key factor in the seismic design of the underground shaft.

- The shaft dynamic displacement is not effected obviously by the different inner water levels. This also indicates that the shaft dynamic response is controlled by surrounding soils.

- The shaft dynamic inner force distribution pattern is mainly determined by surrounding soils, meanwhile the magnitude of the hydrodynamic pressure is nearly the same. Its effect can be neglected compared with the effect of surrounding soils.

Acknowledgements

This research was supported by the National Natural Science Foundation of China (Grant No. 51778464), the Fundamental Research Funds for the Central Universities and "Shuguang Program" supported by Shanghai Education Development Foundation and Shanghai Municipal Education Commission. All supports are gratefully acknowledged.

References

[1] Housner, G. W. (1963) The dynamic behavior of water tanks, *Bulletin of the seismological society of America*, 53(2), 381-387.
[2]Veletsos, A. S.and Shivakumar, P. (1997) Tanks containing liquids or solids. *Computer Analysis and Design of Earthquake Resistant Structures, A Handbook*, 725-774.
[3] Westergaard, H. M. (1933) Water pressures on dams during earthquakes, *Trans. ASCE* **95**, 418-433.
[4] Virella, J. C., Suarez, L. E. and Godoy, L. A. (2005) Effect of pre-stress states on the impulsive modes of vibration of cylindrical tank-liquid systems under horizontal motions, *Modal Analysis* **11**(9), 1195-1220.
[5] Virella, J. C., Godoy, L. A. and Suárez, L. E. (2006) Dynamic buckling of anchored steel tanks subjected to horizontal earthquake excitation, *Journal of Constructional Steel Research* **62**(6), 521-531.
[6] Buratti, N. and Tavano, M. (2014) Dynamic buckling and seismic fragility of anchored steel tanks by the added mass method, *Earthquake Engineering & Structural Dynamics* **43**(1), 1-21.
[7] Livaoglu, R. (2008) Investigation of seismic behavior of fluid–rectangular tank–soil/foundation systems in frequency domain, *Soil Dynamics and Earthquake Engineering* **28**(2), 132-146.
[8] Khanmohammadi, M., Rad, P. L. and Ghalandarzadeh, A. (2017) Experimental study on dynamic behavior of buried concrete rectangular liquid storage tanks using shaking table, *Bulletin of Earthquake Engineering* **15**(9), 3747-3776.
[9] Livaoglu, R., Cakir, T., Dogangun, A. and Aytekin, M. (2011) Effects of backfill on seismic behavior of rectangular tanks, *Ocean Engineering* **38**(10), 1161-1173.
[10] Cakir, T. and Livaoglu, R. (2012) Fast practical analytical model for analysis of backfill-rectangular tank-fluid interaction systems, *Soil Dynamics and Earthquake Engineering* **37**, 24-37.
[11] Kianoush, M. R. and Ghaemmaghami, A. R. (2011) The effect of earthquake frequency content on the seismic behavior of concrete rectangular liquid tanks using the finite element method incorporating soil–structure interaction, *Engineering Structures* **33**(7), 2186-2200.
[12] Ibrahim, R. A. (2005). Liquid sloshing dynamics: theory and applications, Cambridge University Press.
[13] Liu, M. B. and Liu, G. R. (2010) Smoothed particle hydrodynamics (SPH): an overview and recent developments, *Archives of computational methods in engineering* **17**(1), 25-76.
[14] Shao, J. R., Li, H. Q., Liu, G. R. and Liu, M. B. (2012) An improved SPH method for modeling liquid sloshing dynamics, *Computers & Structures* **100**, 18-26.
[15] Mittal, V., Chakraborty, T. and Matsagar, V. (2014) Dynamic analysis of liquid storage tank under blast using coupled Euler-Lagrange formulation, *Thin-Walled Structures* **84**, 91-111.
[16] Tippmann, J., Prasad. S. and Shah, P. (2009) 2-D tank sloshing using the coupled Eulerian-Lagrange (CEL) capability of ABAQUS®/Explicit. *2009 SIMULIA Customer Conference*, Dassault Systemes Simulia Corp.
[17] Rawat, A., Mittal, V., Chakraborty, T. and Matsagar, V. (2019) Earthquake induced sloshing and hydrodynamic pressures in rigid liquid storage tanks analyzed by coupled acoustic-structural and euler-lagrange methods, *Thin-Walled Structures* **134**, 333-346.
[18] Virella, J. C., Prato, C. A. and Godoy, L. A. (2008) Linear and nonlinear 2d finite element analysis of sloshing modes and pressures in rectangular tanks subject to horizontal harmonic motions, *Journal of Sound and Vibration* **312**(3), 442-460.
[19] ABAQUS, (2010) ABAQUS: theory and analysis user's manual, version 6.10. Dassault Systèmes SIMULIA, Providence, RI, USA.